Positronium states in three-dimensional QED

T. W. Allen and C. J. Burden
Department of Theoretical Physics, Research School of Physical Sciences and Engineering, Australian National University, Canberra, Australian Capital Territory 0200, Australia
(Received 21 September 1995)

The e^--e^+ bound state spectrum of three-dimensional QED is investigated in the quenched ladder approximation to the homogeneous Bethe-Salpeter equation with fermion propagators from a rainbow approximation Schwinger-Dyson solution with a variable fermion mass. A detailed analysis of the analytic structure of the fermion propagator is performed so as to test the appropriateness of the methods employed. The large fermion mass limit of the Bethe-Salpeter equation is also considered, including a derivation of the Schrödinger equation, and comparisons are made with existing nonrelativistic calculations.

PACS number(s): 12.20.Ds, 11.10.Kk, 36.10.Dr

I. INTRODUCTION

The similarities between quantum electrodynamics in three space-time dimensions (QED_3) and quantum chromodynamics in four space-time dimensions (QCD_4) and the simplicity of the theory make QED_3 attractive for the study of nonperturbative methods. QED_3 is an Abelian theory and provides a logarithmic confining e^--e^+ potential [1].

Our approach to positronium states in QED_3 is via a solution to the homogenous Bethe-Salpeter equation with fermion propagator input from the Schwinger-Dyson equation. The full Schwinger-Dyson and Bethe-Salpeter equations are intractable. Here we consider a solvable system of integral equations within the quenched ladder approximation. This crude truncation of the full equations does break gauge covariance but has very attractive features and has been employed extensively in QCD_4 spectrum calculations [2,3].

This study continues on from a previous study [4] which uses a four-component fermion version of QED_3. In this version, the massless case exhibits a chiral-like U(2) symmetry broken into a $U(1)\times U(1)$ symmetry by the generation of a dynamical fermion mass, resulting in a doublet of Goldstone bosons. This pionlike solution is important for drawing similarities between QED_3 and QCD_4. The four-component version of QED_3 is also preferred to the two-component version because the Dirac action in the two-component version is not parity invariant for massive fermions. QCD_4 is parity invariant and we aim to have as much in common with that theory as possible.

The previous work was restricted to zero bare fermion mass, while in this study the bare mass is increased from zero to large values in order to compare with results in the nonrelativistic limit. This study also takes a closer look at the choice of fermion propagator input. Knowledge of the analytic properties of the fermion propagator is important for determining the approximation's ability to provide confinement and whether or not any singularities will interfere with a Bethe-Salpeter solution. Based on the work of Maris [5,6] the occurrence of masslike complex singularities is expected which have the potential to influence our calculations.

In Sec. II we look at the Bethe-Salpeter and Schwinger-Dyson approximations used in this work and the method used to find the bound state masses. A brief review of transformation properties in QED_3 is given in the Appendix. These transformation properties are of vital importance for an understanding of the structure of the e^--e^+ vertex function and the classification of the bound states. Section III describes the nonrelativistic limit and the connection between the Bethe-Salpeter and Schrödinger equations for QED_3.

In Sec. IV the approximation to the fermion propagator is detailed. The structure of the propagators will be analyzed in the complex plane where we attempt to locate the expected masslike singularities. In Sec. V the Bethe-Salpeter solutions are reported and comparisons are made with nonrelativistic limit calculations. The results are discussed and conclusions given in Sec. VI.

II. SOLVING THE BETHE-SALPETER EQUATION

The Bethe-Salpeter (BS) kernel for this work is a simple one-photon exchange (ladder approximation) which is a commonly used starting point. For convenience we use the quenched approximation, work in Feynman gauge and work only with the Euclidean metric. Figure 1 shows the Bethe-Salpeter equation in the quenched ladder approximation. The corresponding integral equation is

$$\Gamma(p,P) = -e^2 \int \frac{d^3q}{(2\pi)^3} D(p-q)\,\gamma_\mu S(\tfrac{1}{2}P+q) \times \Gamma(q,P) S(-\tfrac{1}{2}P+q)\,\gamma_\mu , \tag{2.1}$$

where $\Gamma(p,P)$ is the one-fermion irreducible positronium-fermion-antifermion vertex with external legs amputated. The photon propagator $D(p-q)$ in Feynman gauge is $1/(p-q)^2$. The fermion propagator S is the solution to a

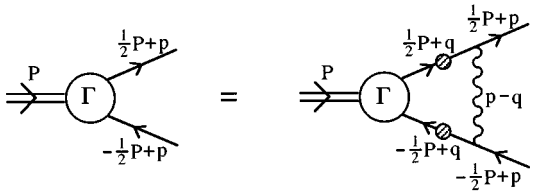

FIG. 1. Diagrammatic representation of Eq. (2.1).

truncated Schwinger-Dyson (SD) equation. A fermion propagator has been chosen which supports spontaneous mass generation necessary for the formation of the Goldstone bosons. The truncated SD equation for a fermion of bare mass m is

$$\Sigma(p)=S(p)^{-1}-(i\not{p}+m)$$
$$=e^2\int\frac{d^3q}{(2\pi)^3}D(p-q)\gamma_\mu S_F(q)\gamma_\mu. \qquad (2.2)$$

This approximation is the quenched, rainbow approximation named so because the photon propagator has been replaced by the bare photon propagator and the vertex function Γ has been replaced by the bare vertex γ, resulting in a series of Feynman diagrams which resemble rainbows. In the quenched approximation the SD and BS equations can be recast in terms of a dimensionless momentum p/e^2 and bare fermion mass m/e^2. From here on we work in dimensionless units and set $e^2=1$.

We use either of the two following equivalent representations of the fermion propagator:

$$S(p)=-i\not{p}\sigma_V(p^2)+\sigma_S(p^2) \qquad (2.3)$$

or

$$S(p)=\frac{1}{i\not{p}A(p^2)+B(p^2)}. \qquad (2.4)$$

The generation of a dynamical fermion mass and the breaking of chiral symmetry is signalled (in the massless limit) by nonzero $B(p^2)$. The vector and scalar parts σ_V and σ_S of the propagator are related to the functions A and B simply by dividing these functions (A,B) by a quantity $p^2A^2(p^2)+B^2(p^2)$.

Note that a substitution of this fermion propagator into the Ward-Takahashi identity shows that the bare vertex approximation breaks gauge covariance. However, this model is simple and does meet the requirement that the appropriate Goldstone bosons are formed [7]. It is not difficult to derive a zero mass solution to our BS equation (BSE) analytically. A vertex proportional to the matrix γ_4 or γ_5, defined in the Appendix, will reduce the quenched ladder BSE to the quenched ladder (rainbow) SD equation (SDE) in the case of zero bound state mass thus forming a doublet of massless states. According to the terminology used in the Appendix this is an axiscalar doublet. These solutions will be seen in Sec. V.

Once the photon and fermion propagators are supplied, the BS equation can be written as a set of numerically tractable integral equations. To do this, we write the BS amplitude Γ in its most general form consistent with the parity and charge conjugation of the required bound state, and then project out the coefficient functions for the individual Dirac components. It is convenient to work in the rest frame of the bound state by setting $P_\mu=(0,0,iM)$. Then the scalar and axiscalar vertices given in the Appendix by Eqs. (A7) and (A9) can be written as

$$\Gamma^S(q,P)=f(q_3,|\mathbf{q}|;M)-\frac{iq_j\gamma_j}{|\mathbf{q}|}U(q_3,|\mathbf{q}|;M)$$
$$+\frac{iq_j^\perp\gamma_j}{|\mathbf{q}|}\gamma_{45}V(q_3,|\mathbf{q}|;M)+i\gamma_3W(q_3,|\mathbf{q}|;M), \qquad (2.5)$$

$$\Gamma^{AS}(q,P)=\begin{pmatrix}\gamma_4\\ \gamma_5\end{pmatrix}f(q_3,|\mathbf{q}|;M)-\frac{iq_j\gamma_j}{|\mathbf{q}|}\begin{pmatrix}\gamma_4\\ \gamma_5\end{pmatrix}U(q_3,|\mathbf{q}|;M)$$
$$+\frac{iq_j^\perp\gamma_j}{|\mathbf{q}|}\begin{pmatrix}\gamma_5\\ -\gamma_4\end{pmatrix}V(q_3,|\mathbf{q}|;M)$$
$$-\gamma_3\begin{pmatrix}\gamma_4\\ \gamma_5\end{pmatrix}W(q_3,|\mathbf{q}|;M), \qquad (2.6)$$

where the index j takes on values 1 and 2 only, $|\mathbf{q}|=(q_1^2+q_2^2)^{1/2}$ and $\mathbf{q}^\perp=(-q_2,q_1)$. The pseudoscalar and axipseudoscalar vertices are obtained from the scalar and axiscalar vertices by multiplication by the matrix γ_{45}.

It is found that the same coupled integral equations result when a vertex is multiplied by the matrix γ_{45} and so (scalar, pseudoscalar) and (axiscalar, axipseudoscalar) form two pairs of degenerate states.

The four equations derived from the BSE, after some manipulation including an angular integration, are [4]

$$f(p)=\frac{3}{(2\pi)^2}\int_{-\infty}^{\infty}dq_3\int_0^\infty|\mathbf{q}|d|\mathbf{q}|\frac{1}{(\alpha^2-\beta^2)^{1/2}}$$
$$\times[T_{ff}f(q)+T_{fU}U(q)+T_{fV}V(q)+T_{fW}W(q)],$$
$$U(p)=\frac{1}{(2\pi)^2}\int_{-\infty}^{\infty}dq_3\int_0^\infty|\mathbf{q}|d|\mathbf{q}|\frac{(\alpha^2-\beta^2)^{1/2}-\alpha}{\beta(\alpha^2-\beta^2)^{1/2}}$$
$$\times[T_{Uf}f(q)+T_{UU}U(q)+T_{UV}V(q)+T_{UW}W(q)],$$
$$V(p)=\frac{1}{(2\pi)^2}\int_{-\infty}^{\infty}dq_3\int_0^\infty|\mathbf{q}|d|\mathbf{q}|\frac{(\alpha^2-\beta^2)^{1/2}-\alpha}{\beta(\alpha^2-\beta^2)^{1/2}}$$
$$\times[T_{Vf}f(q)+T_{VU}U(q)+T_{VV}V(q)+T_{VW}W(q)],$$
$$W(p)=\frac{1}{(2\pi)^2}\int_{-\infty}^{\infty}dq_3\int_0^\infty|\mathbf{q}|d|\mathbf{q}|\frac{1}{(\alpha^2-\beta^2)^{1/2}}$$
$$\times[T_{Wf}f(q)+T_{WU}U(q)+T_{WV}V(q)+T_{WW}W(q)], \qquad (2.7)$$

where

$$\alpha=(p_3-q_3)^2+|\mathbf{p}|^2+|\mathbf{q}|^2,\quad \beta=-2|\mathbf{p}||\mathbf{q}|.$$

Now define the momentum Q by

$$Q^2=q_3^2+|\mathbf{q}|^2-\frac{1}{4}M^2+iMq_3, \qquad (2.8)$$

and use the abbreviations $\sigma_V=\sigma_V(Q^2)$ and $\sigma_S=\sigma_S(Q^2)$ for use in the definition of the functions $T_{ff},T_{fU},\ldots$ which are analytic functions of $q_3,|\mathbf{q}|$, and M. The diagonal T's are given by

$$T_{ff}=(\tfrac{1}{4}M^2+q_3^2+|\mathbf{q}|^2)|\sigma_V|^2\mp|\sigma_S|^2,$$

$$T_{UU}=(\tfrac{1}{4}M^2+q_3^2-|\mathbf{q}|^2)|\sigma_V|^2\pm|\sigma_S|^2,$$

$$T_{VV}=(\tfrac{1}{4}M^2+q_3^2+|\mathbf{q}|^2)|\sigma_V|^2\pm|\sigma_S|^2,$$

$$T_{WW}=-(\tfrac{1}{4}M^2+q_3^2-|\mathbf{q}|^2)|\sigma_V|^2\pm|\sigma_S|^2, \qquad (2.9)$$

where the upper sign applies to the scalar equations and the lower sign to the axiscalar equations. The off-diagonal T's are, for the scalar positronium states,

$$T_{fU}=T_{Uf}=(\sigma_V^*\sigma_S+\sigma_S^*\sigma_V)|\mathbf{q}|,$$

$$T_{fV}=T_{Vf}=-M|\mathbf{q}||\sigma_V|^2,$$

$$T_{fW}=T_{Wf}=-(\sigma_V^*\sigma_S+\sigma_S^*\sigma_V)q_3+\frac{i}{2}(\sigma_V^*\sigma_S-\sigma_S^*\sigma_V)M,$$

$$T_{UV}=T_{VU}=-[\tfrac{1}{2}(\sigma_V^*\sigma_S+\sigma_S^*\sigma_V)M+iq_3(\sigma_V^*\sigma_S-\sigma_S^*\sigma_V)],$$

$$T_{UW}=T_{WU}=2q_3|\mathbf{q}||\sigma_V|^2,$$

$$T_{VW}=T_{WV}=-i(\sigma_V^*\sigma_S-\sigma_S^*\sigma_V)|\mathbf{q}|, \qquad (2.10)$$

and, for the axiscalar states,

$$T_{fU}=T_{Uf}=i(\sigma_V^*\sigma_S-\sigma_S^*\sigma_V)|\mathbf{q}|,$$

$$T_{fV}=-T_{Vf}=M|\mathbf{q}||\sigma_V|^2,$$

$$T_{fW}=-T_{Wf}=-i(\sigma_V^*\sigma_S-\sigma_S^*\sigma_V)q_3-\tfrac{1}{2}(\sigma_V^*\sigma_S+\sigma_S^*\sigma_V)M,$$

$$T_{UV}=T_{VU}=-\left[\frac{i}{2}(\sigma_V^*\sigma_S-\sigma_S^*\sigma_V)M-q_3(\sigma_V^*\sigma_S+\sigma_S^*\sigma_V)\right],$$

$$T_{UW}=-T_{WU}=-2q_3|\mathbf{q}||\sigma_V|^2,$$

$$T_{VW}=-T_{WV}=(\sigma_V^*\sigma_S+\sigma_S^*\sigma_V)|\mathbf{q}|. \qquad (2.11)$$

This is the same set of equations solved in Ref. [4] with only the fermion propagator input altered. The bare fermion mass m only comes into the calculation through this input.

The solution to the BSE involves iteration of the coupled integral equations in Eq. (2.7). These equations may be rewritten as

$$\mathbf{f}(|\mathbf{p}|,p_3;M)=\int dq_3\int d|\mathbf{q}|K(|\mathbf{p}|,p_3;|\mathbf{q}|,q_3;M)\mathbf{f}(|\mathbf{q}|,q_3;M), \qquad (2.12)$$

where $\mathbf{f}=(f,U,V,W)^T$. For each symmetry case and each fermion mass this is solved as an eigenvalue problem of the form

$$\int dqK(p,q;M)\mathbf{f}(q)=\Lambda(M)\mathbf{f}(p), \qquad (2.13)$$

for a given test mass M. This is repeated for different test bound state masses until an eigenvalue $\Lambda(M)=1$ is obtained.

III. NONRELATIVISTIC LIMIT

We consider now the nonrelativistic limit $m\to\infty$ of our BS formalism in order to enable comparisons with existing numerical calculations [8,9] of the Schrödinger equation for QED_3, and with the large m solution of Eq. (2.7)

The Schrödinger equation with a confining logarithmic potential is an interesting problem in its own right. Initially one is faced with the problem of setting the scale of the potential, or equivalently, setting the zero of energy of the confined bound states. A solution to this problem was proposed by Sen [10] and Cornwall [11] in terms of cancellation of infrared divergences in perturbation theory. They introduce a regulating photon mass μ in order to set the potential as the two-dimensional Fourier transform of the photon propagator $1/(k^2+\mu^2)$, leading to a potential proportional to $\ln(\mu r)$. They further interpret the sum of the bare fermion mass and the fermion self-energy evaluated at the bare fermion mass shell as a renormalized fermion mass, leading to a mass renormalisation $\delta m\propto\ln(m/\mu)$. The logarithmic divergences in the photon potential and the fermion self-energy then conspire to cancel leaving a finite positronium mass.

The first numerical treatment of the Schrödinger equation for QED_3 using this line of argument was carried out by Yung and Hamer [8]. In a subsequent, improved calculation by Tam, Hamer, and Yung [9], the formalism was shown to be consistent with an analysis of QED_3 from the point of view of discrete light cone quantization. Their resulting expression for the bound state energy, obtained as a solution to the differential equation

$$\left\{-\frac{1}{m}\nabla^2+\frac{1}{2\pi}[C+\ln(mr)]\right\}\phi(\mathbf{r})=(E-2m)\phi(\mathbf{r}), \qquad (3.1)$$

where C is Euler's constant, is given in terms of the bare fermion mass m as

$$E=2m+\frac{1}{4\pi}\ln m+\frac{1}{2\pi}\left(\lambda-\frac{1}{2}\ln\frac{2}{\pi}\right). \qquad (3.2)$$

The lightest s-wave positronium state and first exited state are given by $\lambda_0=1.7969$ and $\lambda_1=2.9316$, respectively. The first five states are provided in [9].

Here we present a treatment of the nonrelativistic limit of the QED_3 positronium spectrum in terms of our SD-BS equation formalism. We begin with the fermion propagator in the limit $m\to\infty$. For large fermion mass we expect the residual effect of the chiral symmetry-breaking contribution to

the fermion self-energy to be small compared with contribution from the perturbative loop expansion. We shall therefore assume to begin with that the self-energy is reasonably well approximated by the one-loop result. The validity of this approximation for spacelike momenta will be demonstrated numerically in the next section.

The one-loop fermion self energy, with the functions A and B defined in Eq. (2.4), is given by

$$A=1+\frac{\Sigma_A(p^2/m^2)}{m}, \tag{3.3}$$

where

$$\Sigma_A(x^2)=\frac{1}{8\pi x^2}\left[1-\frac{1-x^2}{2x}\arccos\left(\frac{1-x^2}{1+x^2}\right)\right], \tag{3.4}$$

and

$$B=m\left(1+\frac{\Sigma_B(p^2/m^2)}{m}\right), \tag{3.5}$$

where

$$\Sigma_B(x^2)=\frac{3}{8\pi x}\arccos\left(\frac{1-x^2}{1+x^2}\right). \tag{3.6}$$

This result is valid for (Euclidean) spacelike momenta $p^2>0$. An analytic continuation of the Σ functions valid for $|p^2|<m^2$, or $|x|<1$, is

$$\Sigma_A(x^2)=\frac{1}{8\pi i x}\left[\frac{x^2-1}{2x^2}\ln\left(\frac{1+ix}{1-ix}\right)+\frac{i}{x}\right], \tag{3.7}$$

$$\Sigma_B(x^2)=\frac{3}{8\pi i x}\ln\left(\frac{1+ix}{1-ix}\right). \tag{3.8}$$

Note that this representation exposes a logarithmic infinity in the self-energy at the bare fermion mass pole $p^2=-m^2$. This is the infrared divergence in the renormalized fermion self-energy as defined by Sen [10] referred to above. However, in our formalism, this singularity does not lead to a pole

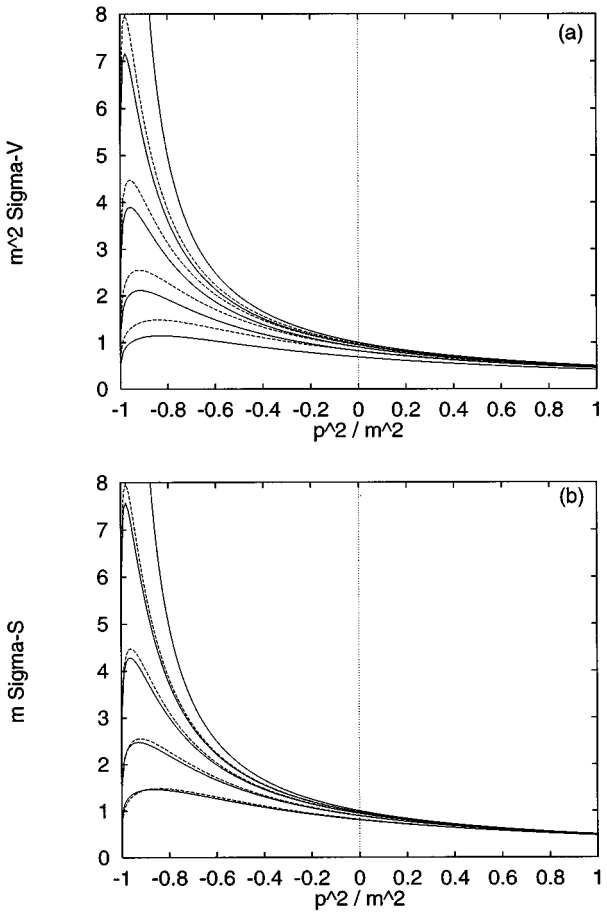

FIG. 2. (a) and (b) show one-loop approximations using Eqs. (2.3), (2.4), and (3.3)–(3.6) for $m^2\sigma_V$ and $m\sigma_S$, respectively (solid lines). These are compared with the vector and scalar parts of the approximation Eq. (3.14) (dashed lines). The curves are drawn for fermion masses (from bottom to top) 1, 2, 4, 8, and ∞.

in the propagator functions σ_V and σ_S defined in Eq. (2.3), which would signal the propagation of a free fermion [12], but a logarithmic zero.

Using Eqs. (3.3) and (3.5) we obtain

$$\sigma_V(p^2)=\frac{1}{m^2}\,\frac{1+\Sigma_A/m}{\epsilon(1+\Sigma_A/m)^2+2[1+(\Sigma_A+\Sigma_B)/2m](\Sigma_B-\Sigma_A)/m}, \tag{3.9}$$

$$\sigma_S(p^2)=\frac{1}{m}\,\frac{1+\Sigma_B/m}{\epsilon(1+\Sigma_A/m)^2+2[1+(\Sigma_A+\Sigma_B)/2m](\Sigma_B-\Sigma_A)/m}, \tag{3.10}$$

where we have defined

$$\epsilon=\frac{p^2+m^2}{m^2}. \tag{3.11}$$

The functions σ_V and σ_S are plotted in Figs. 2(a) and 2(b) for $m=$ 1, 2, 4, 8, and ∞, the final curve being the bare propagator. From these plots we see that for large m, the deviation from the bare propagator due to the one-loop self-energy is dominated by the logarithmic contribution near the bare fermion mass shell, $\epsilon=0$. With this in mind, we shall use the approximation

$$\Sigma_A(x^2)\approx-\frac{1}{8\pi}\ln\frac{\epsilon}{4}, \tag{3.12}$$

$$\Sigma_B(x^2)\approx -\frac{3}{8\pi}\ln\frac{\epsilon}{4}. \tag{3.13}$$

Taking ϵ to be of order $1/m$ for the purposes of the BS equation [see Eq. (3.16) below] these approximations give

$$S(p)=\frac{-i\not{p}+m}{m}\frac{1}{m\epsilon-(1/2\pi)\ln(\epsilon/4)}\left[1+O\left(\frac{\ln m}{m}\right)\right]. \tag{3.14}$$

The vector and scalar parts of this approximate propagator [without the $O(\ln m/m)$ corrections] are also plotted in Figs. 2(a) and 2(b) for comparison.

Turning now to the BS equation, we set the bound state momentum in Eq. (2.1) equal to $P_\mu=(2m+\delta)iv_\mu$, where $v_\mu=(0,0,1)$ and $-\delta$ is a ''binding energy.'' This gives (according to the momentum distribution in Fig. 1)

$$\Gamma(p)=-\int\frac{d^3q}{(2\pi)^3}D(p-q)\gamma_\mu S\left[-\left(m+\frac{\delta}{2}\right)iv_\mu+q_\mu\right]\Gamma(q)S\left[\left(m+\frac{\delta}{2}\right)iv_\mu+q_\mu\right]\gamma_\mu. \tag{3.15}$$

Setting

$$\epsilon=\frac{2}{m}\left(-\frac{1}{2}\delta+iq_3+\frac{|\mathbf{q}|^2}{2m}\right)+O\left(\frac{1}{m^2}\right) \tag{3.16}$$

in Eq. (3.14) gives

$$S\left[\left(m+\frac{\delta}{2}\right)iv_\mu+q_\mu\right]=\frac{1+\gamma_3}{2}\frac{1}{[-(1/2)\delta+iq_3+|\mathbf{q}|^2/2m]-(1/4\pi)\ln(\epsilon/4)}+O\left(\frac{\ln m}{m}\right). \tag{3.17}$$

Similarly

$$S\left[-\left(m+\frac{\delta}{2}\right)iv_\mu+q_\mu\right]=\frac{1-\gamma_3}{2}\frac{1}{[-(1/2)\delta-iq_3+|\mathbf{q}|^2/2m]-(1/4\pi)\ln(\epsilon^*/4)}+O\left(\frac{\ln m}{m}\right). \tag{3.18}$$

The $|\mathbf{q}|^2/2m$ term has been retained here to ensure convergence of the $|\mathbf{q}|$ integral in the BS equation below. Since the vertex Γ is defined with the fermion legs truncated, and $S\propto(1/2)(1\pm\gamma_3)$, the only relevant part of Γ is the projection $(1/2)\times(1-\gamma_3)\Gamma(1/2)(1+\gamma_3)$. With this in mind, the general forms in Eqs. (2.5) and (2.6) become

$$\begin{aligned}\frac{1}{2}(1-\gamma_3)\Gamma^S\frac{1}{2}(1+\gamma_3)&=\frac{1}{2}(1-\gamma_3)\frac{q_j\gamma_j}{|\mathbf{q}|}g(q_3,|\mathbf{q}|),\\ \frac{1}{2}(1-\gamma_3)\Gamma^{AS}\frac{1}{2}(1+\gamma_3)&=\frac{1}{2}(1-\gamma_3)\begin{pmatrix}\gamma_4\\ \gamma_5\end{pmatrix}g(q_3,|\mathbf{q}|).\end{aligned} \tag{3.19}$$

Substituting Eqs. (3.17), (3.18), and (3.19) into Eq. (3.15) one obtains, for the scalar states the single integral equation

$$g(p)\approx\int\frac{d^3q}{(2\pi)^3}\frac{1}{(p-q)^2}\frac{\mathbf{p}\cdot\mathbf{q}}{|\mathbf{p}||\mathbf{q}|}\frac{g(q)}{|-(1/2)\delta+iq_3+|\mathbf{q}|^2/2m-(1/4\pi)\ln(1/2m)[-(1/2)\delta+iq_3+|\mathbf{q}|^2/2m]|^2}, \tag{3.20}$$

and, for the axiscalar states the single equation,

$$g(p)\approx\int\frac{d^3q}{(2\pi)^3}\frac{1}{(p-q)^2}\frac{g(q)}{|-(1/2)\delta+iq_3+|\mathbf{q}|^2/2m-(1/4\pi)\ln(1/2m)[-(1/2)\delta+iq_3+|\mathbf{q}|^2/2m]|^2}. \tag{3.21}$$

Note that, without the $|\mathbf{q}|^2/2m$ term in the denominator, translation invariance of the integrand implies that g is independent of $|\mathbf{q}|$. In reality, g is a slowly varying function of $|\mathbf{q}|$, and this extra $O(1/m^2)$ term must be retained in ϵ to account for the fact that the relevant region of integration in Eqs. (3.20) and (3.21) extends out to $O(\sqrt{m})$ in the $|\mathbf{q}|$ direction, but only $O(1)$ in the q_3 direction. Numerical solutions of Eqs. (3.20) and (3.21) will be given in Sec. V. The function g is an even or odd function of q_3 corresponding to positronium states which are even or odd, respectively, under charge conjugation.

In order to obtain a Schrödinger equation, we now rewrite the axiscalar equation in the form

$$g(p)=\int \frac{d^2\mathbf{q}}{(2\pi)^2}\int_{-\infty}^{\infty}\frac{dq_3}{2\pi}\,\frac{1}{(p_3-q_3)^2+|\mathbf{p}-\mathbf{q}|^2}$$

$$\times\frac{g(q)}{[-(1/2)\delta+iq_3+|\mathbf{q}|^2/2m+\Sigma_+(q_3,|\mathbf{q}|)][-(1/2)\delta-iq_3+|\mathbf{q}|^2/2m+\Sigma_-(q_3,|\mathbf{q}|)]}, \tag{3.22}$$

where

$$\Sigma_\pm(q_3,|\mathbf{q}|)=-\frac{1}{4\pi}\ln\left[\frac{1}{2m}\left(-\frac{1}{2}\delta\pm iq_3+\frac{|\mathbf{q}|^2}{2m}\right)\right]. \tag{3.23}$$

Assuming the integrand dies off sufficiently rapidly as $q_3\to -i\infty$, we deform the contour of integration around the pole at

$$q_3^{\text{pole}}=-i\left(-\frac{1}{2}\delta+\frac{|\mathbf{q}|^2}{2m}+\Sigma_-(q_3^{\text{pole}},|\mathbf{q}|)\right), \tag{3.24}$$

to obtain

$$g(p)=\int \frac{d^2\mathbf{q}}{(2\pi)^2}\,\frac{1}{(p_3-q_3^{\text{pole}})^2+|\mathbf{p}-\mathbf{q}|^2}\,\frac{g(q_3^{\text{pole}},|\mathbf{q}|)}{-\delta+|\mathbf{q}|^2/m+2\ \mathrm{Re}\Sigma_-(q_3^{\text{pole}},|\mathbf{q}|)}. \tag{3.25}$$

(We could equally well deform the contour around the pole at $(q_3^{\text{pole}})^*$ if the integrand decays in the opposite direction, without affecting our final result.)

Defining

$$\Phi(p_3,|\mathbf{p}|)=\frac{g(p_3,|\mathbf{p}|)}{-\delta+|\mathbf{p}|^2/m+2\ \mathrm{Re}\Sigma_-(p_3,|\mathbf{p}|)}, \tag{3.26}$$

gives

$$\left\{-\delta+\frac{|\mathbf{p}|^2}{m}+2\ \mathrm{Re}\Sigma_-(p_3,|\mathbf{p}|)\right\}\Phi(p_3,|\mathbf{p}|)=\int\frac{d^2\mathbf{q}}{(2\pi)^2}\,\frac{1}{(p_3-q_3^{\text{pole}})^2+|\mathbf{p}-\mathbf{q}|^2}\,\Phi(q_3^{\mathbf{pole}},|\mathbf{q}|). \tag{3.27}$$

In order to isolate the logarithmic infrared divergence we set

$$p_3=p_3^{\text{pole}}+\mu, \tag{3.28}$$

with μ small and real, and p_3^{pole} defined by analogy with Eq. (3.24). The right-hand side (RHS) of Eq. (3.27) then becomes

$$\mathrm{RHS}=\int\frac{d^2\mathbf{q}}{(2\pi)^2}\,\frac{1}{\mu^2+O[\mu(|\mathbf{p}|-|\mathbf{q}|)]+|\mathbf{p}-\mathbf{q}|^2}\,\phi(\mathbf{q})=\text{FT of }\ \frac{-1}{2\pi}\left[C+\ln\left(\frac{\mu r}{2}\right)\right]\phi(\mathbf{r})\ \ \text{as}\ \ \mu\to 0, \tag{3.29}$$

where $\phi(\mathbf{q})=\Phi(q_3^{\mathbf{pole}},|\mathbf{q}|)$, FT denotes the Fourier transform, and C is Euler's constant.

Following the reasoning of [10,11], this logarithmic divergence should be cancelled by the fermion self-energy contribution $2\mathrm{Re}\Sigma_-(p_3,|\mathbf{p}|)$. However, from Eq. (3.23), we see that the logarithmic divergence in the self-energy occurs at the bare fermion mass pole $p_3^{\text{bare}}=-i(-\delta/2+|\mathbf{p}|^2/2m)$, and not the dressed pole $p_3^{\mathbf{pole}}$. The problem lies in the use of the one-loop approximation. If instead the fermion self-energy is calculated to all orders in rainbow approximation, the self-energy feeds back into the loop integral via the propagator to replace Eq. (3.23) by

$$\Sigma_-(p_3,|\mathbf{p}|)=-\frac{1}{4\pi}\ln\left[\frac{1}{2m}\left(-\frac{1}{2}\delta-ip_3+\frac{|\mathbf{p}|^2}{2m}+\Sigma_-(p_3,|\mathbf{p}|)\right)\right], \tag{3.30}$$

which provides a rainbow SD equation for Σ_- in the nonrelativistic limit. Then using Eqs. (3.27), (3.24), (3.28), (3.29), and (3.30) and Fourier transforming we finally obtain

$$\left\{-\frac{1}{m}\nabla^2+\frac{1}{2\pi}[C+\ln(mr)]\right\}\phi(\mathbf{r})=\delta\phi(\mathbf{r}), \tag{3.31}$$

agreeing with Eq. (3.1). Had we started from the scalar equation (3.20) in place of the axiscalar equation, the same result would have been obtained at Eq. (3.29), leading to an identical Schrödinger equation.

The important point to notice in this derivation is the significance of a non-perturbative solution to the SD equation in canceling the infrared divergences. In the massless fermion limit, it is well known that chiral symmetry breaking plays a pivotal role in determining the bound state spectrum. It appears also that, even in the nonrelativistic limit, the remnant effects of chiral symmetry breaking, via a non-perturbative solution to the SD equation, have a role to play.

IV. THE FERMION PROPAGATOR

The BSE described in Sec. II requires a fermion propagator input in the form of Eq. (2.3) or Eq. (2.4) and this needs to be available over a region in the complex p^2 plane defined by Eq. (2.8) for q_3 and $|\mathbf{q}|$ real. This is the region [13,3]

$$\Omega=\left\{ Q^2=X+iY \middle| X>\frac{Y^2}{M^2}-\frac{1}{4}M^2 \right\}. \tag{4.1}$$

In this section we investigate ways of obtaining a solution to the SDE over Ω. The fermion propagator, and thus the functions σ_V and σ_S, must be well behaved over this region.

The solution to the SDE (2.2) is quite simple along the positive real (spacelike) p^2 axis. Substitution of the general expression for the fermion propagator (2.4) into the SDE gives an integral equation involving A and B functions which can be split into two coupled integral equations by simple projections. Angular integrations can be performed to leave one-dimensional integrals (over the modulus of the q vector):

$$A(p^2)-1=\frac{1}{4\pi^2p^2}\int_0^\infty dq\,\frac{qA(q^2)}{q^2A^2(q^2)+B^2(q^2)}\left(\frac{p^2+q^2}{4p}\ln\left(\frac{p+q}{p-q}\right)^2-q\right),$$

$$B(p^2)-m=\frac{3}{8\pi^2p}\int_0^\infty dq\,\frac{qB(q^2)}{q^2A^2(q^2)+B^2(q^2)}\ln\left(\frac{p+q}{p-q}\right)^2. \tag{4.2}$$

The integrations range from 0 to some UV cutoff along the positive real axis. This theory is superrenormalizable and thus has no ultraviolet divergences and so this cutoff is merely a numerical limit made large enough so that it has no bearing on the results.

For a set of points p corresponding to the set of q points in the integration, the equations are iterated until convergence to leave the solution along the positive real axis. However, the solution is required for complex p^2. We see three possibilities. The first is to use the converged functions $A(q^2)$ and $B(q^2)$ in the integrals over the same contour (positive real q^2) and supply the complex point p desired. The integrals should provide the solution at that point p. However the analytic structure of the integrands in Eq. (4.2) will not allow an analytic continuation by this method, because a pinch singularity in the integrand forces us to integrate through the point p [6].

The second possibility is to rotate the contour through an angle 2ϕ in the p^2 plane so that it passes through the desired point p [13]. In this way a cancellation of the complex parts within the logarithms occurs. Figure 3 shows the first and second contours (C_1 and C_2, respectively). It can be seen from Eq. (4.2) that the logarithms will have real arguments along the radial portion of C_2, while the arc portion contributes nothing to the integral because the integrand falls off sufficiently quickly in the ultraviolet [6].

Based on the Landau gauge calculations of Maris [5,6] we expect conjugate singularities to occur in the second and third quadrants of the p^2 plane away from the negative real (timelike) axis. Thus, as 2ϕ increases towards π from zero (and the negative real p^2 axis is approached) a singularity interferes and we may have convergence problems. It will be seen that these singularities can lie a fair way from $\phi=\pi/2$ and convergence problems can occur for ϕ not much more than $\pi/4$ (i.e., barely reaching into the second quadrant of p^2). For the case $m=0$ to be considered shortly, no solution could be found for ϕ greater than 0.90 rad (with a reasonable convergence criterion $\Delta B/B<0.001$). For this solution to be applied to the BSE we need to know the value of the fermion propagator for ϕ from 0 to $\pi/2$ and so this method is not practical. However, although a slowing of convergence as ϕ increases prevents a solution being attained in all of Ω, it does provide an accurate solution in a large portion of Ω. We therefore have a test for any A and B functions we wish to use in the BSE.

The third possibility, and the one employed here and in [4], is to find a good analytic fit along the positive real p^2

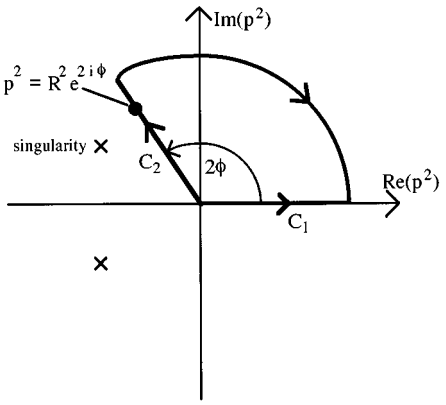

FIG. 3. The first and second (deformed) contours of integration C_1 and C_2 for solution to Eq. (4.2).

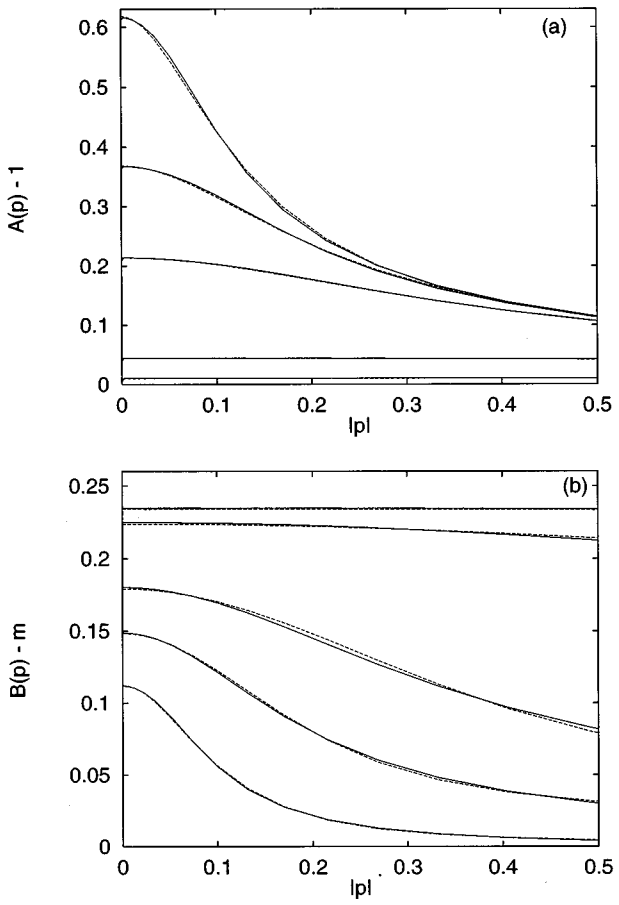

FIG. 4. (a) compares the SDE solutions and fitting functions for $A-1$ for fermion masses (from top to bottom) $m=0$, 0.025, 0.1, 1, and 5. (b) shows $B-m$ for fermion masses (from bottom to top) $m=0$, 0.025, 0.1, 1, and 5.

axis and extend the solution into the complex plane by analytic continuation. These fits may be for A and B or for the functions σ_V and σ_S. The work of Maris [6] suggests that it is not necessary for σ_V and σ_S to be entire functions for the fermions to be confined, only that there be no poles on the timelike p^2 axis. Fits to functions A and B used in previous work [4] based on the known asymptotic infrared and ultraviolet behavior of these functions were tested by comparing them with the direct solution for various angles ϕ. The fits, adjusted to allow variable fermion mass m, are given by

$$A_{\text{fit}}(p^2)=\frac{a_1}{(a_2^2+p^2)^{1/2}}+a_3e^{-a_4p^2}+1,$$

$$B_{\text{fit}}(p^2)=\frac{b_1}{b_2+p^2}+b_3e^{-b_4p^2}+m. \tag{4.3}$$

The parameters a_n, b_n are functions of fermion mass. The numerical solution to which these functions were fitted is an iterative solution to the SDE using a nonuniform 51-point grid along the positive real axis up to a momentum cutoff $p=1000$ using a 0.1% tolerance in the integration routine. Plots of the numerical solutions and function fits for various m values are given in Fig. 4.

TABLE I. Conjugate singularities for fermion propagator fit and corresponding limits on bound state mass for fermion masses from 0 to 5.0.

m	p^2	$M_{\max}$
0.000	$-0.0034 \pm i\ 0.0057$	0.142
0.001	$-0.0041 \pm i\ 0.0064$	0.153
0.004	$-0.0060 \pm i\ 0.0086$	0.182
0.009	$-0.0081 \pm i\ 0.0140$	0.206
0.016	$-0.0121 \pm i\ 0.0192$	0.247
0.025	$-0.0216 \pm i\ 0.0260$	0.325
0.036	$-0.0314 \pm i\ 0.0345$	0.386
0.049	$-0.0468 \pm i\ 0.0387$	0.464
0.064	$-0.0618 \pm i\ 0.0417$	0.522
0.081	$-0.0815 \pm i\ 0.0440$	0.590
0.1	$-0.0647 \pm i\ 0.0000$	0.509
0.5	$-0.4894 \pm i\ 0.0000$	1.399
1	$-1.4260 \pm i\ 0.0000$	2.388
2	$-4.8925 \pm i\ 0.0000$	4.424
3	$-10.3776 \pm i\ 0.0000$	6.443
4	$-17.9613 \pm i\ 0.0000$	8.476
5	$-27.3616 \pm i\ 0.0000$	10.462

Note that it is the σ functions that are important in Eq. (2.1) and not A and B, and thus the effect of the fit on the denominator $p^2A^2+B^2$ relating these must be considered. Conjugate poles exist where the factor $p^2A^2+B^2$ appearing in the denominator of the BSE integrand is zero. Table I lists the conjugate poles arising from the fits for each fermion mass and the corresponding maximum bound state masses allowed. The maximum M allowed is the value for which the boundary of Ω in Eq. (4.1) coincides with the conjugate poles. No comment about the viability of our model BSE can be made until solutions are attempted because the integration region depends on the solution mass M.

The location of the conjugate singularities for the $m=0$ case in Table I is slightly different to that reported in Ref. [4] where it is $-0.004\,00\pm i0.006\,66$. This is because of the flexibility of the fitting functions. The fit in this work and that in Ref. [4] for the zero-fermion mass case had similar accuracy along the positive real p^2 axis but had the freedom to take on slightly different forms throughout the complex plane. This is because along the positive real p^2 axis the nonasymptotic form fixing parameters (a_4 and b_4) are only loosely determined. Despite the difference in the two results, the BSE calculation for bound state masses should show close agreement as each fit adequately models the direct solution throughout the complex plane.

The singularities in the σ fits for fermion masses greater than or equal to 0.1 lie on the negative real p^2 axis. This suggests that free propagation occurs at these masses and the model is not confining. An accurate location of the singularities in the SDE solution would be needed before it can be said whether this result is due to the fits or the rainbow approximation used in the SDE solution. According to Ref. [6] the rainbow approximation SDE solution is expected to be confining even for large fermion mass. Thus we assume our result is due to the lack of accuracy in our fits near the negative real p^2 axis and that it is likely that the singularities

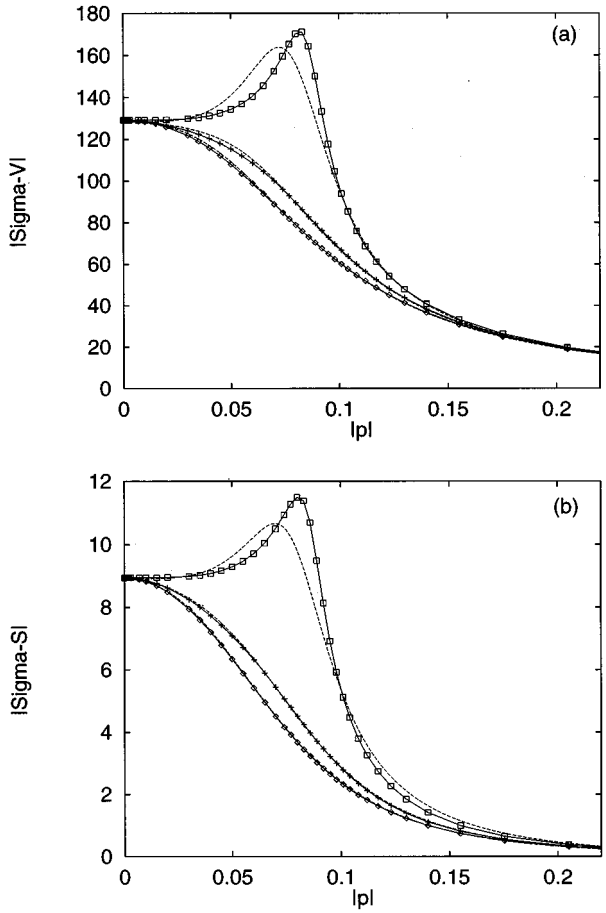

FIG. 5. (a) and (b) show SDE solutions and function fits for σ_V and σ_S respectively for fermion mass 0 with angles $\phi=0$ ($\diamond$), $\pi/8$ ($+$), and $\pi/4$ ($\square$).

move close to that axis as m increases but never actually lie on that axis.

Figures 5(a) and 5(b) show plots of σ_V and σ_S moduli, respectively, for zero-fermion mass and angles $\phi=0$, $\phi=\pi/8$, and $\phi=\pi/4$ against the p modulus (with a range far smaller than the UV cutoff used in our calculations). The direct solutions to the SDE and the fits are compared. It can be seen that the functions are very good fits along the positive real axis ($\phi=0$), where both σ_V and σ_S are real. The fit is also good for $\phi=\pi/8$. Real and imaginary components have not been given separately as they show similar agreement. In the case $\phi=\pi/4$ the fitting function has begun to deviate from the SDE solution. This is mostly due to the apparent difference in the location of a spike. Based on the largest bound state mass for $m=0$ reported in the next section, the BSE integration region Ω extends along the direction $\phi=\pi/4$ out to a modulus of approximately 0.083. In this range the small angle solutions are very accurate but for larger ϕ, much of the error due to the difference in the location of the spike will be experienced. As the angle is increased further convergence problems occur until eventually no solution can be found at all ($\phi>0.90$).

The spike forming in these plots signals that, as ϕ is increased, the contour of integration approaches a singularity. In fact, the conjugate poles which lie just off (or on as is the case for larger m) the negative real p^2 axis ($\phi=\pi/2$) are approached. It is important that both the direct solution to the SDE and the fits used in this work have this feature. This spike was not seen in any other fits which we attempted. Based on Fig. 5 it seems clear that the direct solution to the SDE must have singularities close to those in the fitting functions.

Because the spikes are not in exactly the same places some error will be introduced in the contributions from the large ϕ part of Ω. When the bound state mass becomes large, the large ϕ contributions will become more important and thus we expect the error in the position of the spikes to result in some noise in the solutions to the BS equation for large fermion mass.

The σ functions were studied for all fermion masses used in this work in the same fashion. The results were similar to the $m=0$ case and need not be shown here. In each case, when ϕ was increased far enough, a spike was observed in both the fit and solution, after which lack of convergence prevented an SDE solution.

However, for very large fermion masses, the accuracy of the fits decreases as m increases, and with good reason. As m tends to infinity, the functions A and B approach constants (1 and m, respectively). For moderately large fermion masses experienced in this work, these functions become almost constant along the positive real p^2 axis while having a singularity near the negative real p^2 axis. It is too much to ask for simple four parameter fits along the positive real p^2 axis to reproduce accurately complex behavior deep into the real timelike p^2 axis. The one-loop propagators, Fig. 2 described in Sec. III illustrate this well. There one can see how smooth and level the σ functions are along the positive real p^2 axis and also how steep the functions become back along the negative real p^2 axis.

Before moving on to the next section, we return briefly to the one-loop approximation to the fermion propagator necessary for the non-relativistic approximations described in Sec. III. Figure 6(a) compares our rainbow approximation solution A to the one-loop result given in Eqs. (3.3) and (3.4). Figure 6(b) compares B from our rainbow approximation solution and the result in Eqs. (3.5) and (3.6). Both of these comparisons were made at a large fermion mass ($m=5$). It can be seen that the curves in each case are in reasonable agreement, at least for spacelike momenta.

V. NUMERICAL SOLUTION OF THE BETHE-SALPETER EQUATION

The fits given by Eq. (4.3) to the fermion propagator for a range of fermion masses were used in the solution of the Bethe-Salpeter coupled integral equations Eq. (2.7). This problem was restated in Eq. (2.13) as an eigenvalue problem.

A grid of 25×25 ($|\mathbf{q}|,q_3$) tiles were used for the iterative procedure with linear interpolation on each of those tiles used for the sums ($T_{ij}f_j$) which are supplied at the corners of the tiles from the previous iteration. The tiles were nonuniform in size and an upper limit to the momentum components ($|\mathbf{q}|$ and q_3) of between 3.0 and 9.0 was used. The equations were iterated to convergence each time to determine eigenvalues for a given test bound state mass M. The bound state masses were located by repetitive linear interpolation or extrapolation to search for the point where the ei-

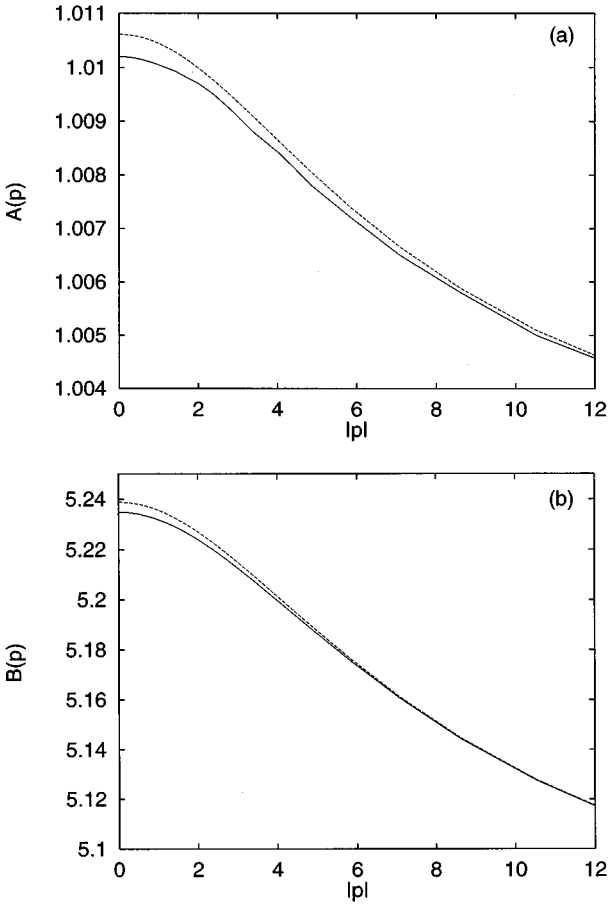

FIG. 6. (a) compares the function $A(p^2)$ from the rainbow SDE calculation (solid curve) and the one-loop result (dashed curve) and (b) compares $B(p^2)$ results along the positive real p axis for fermion mass $m=5.0$.

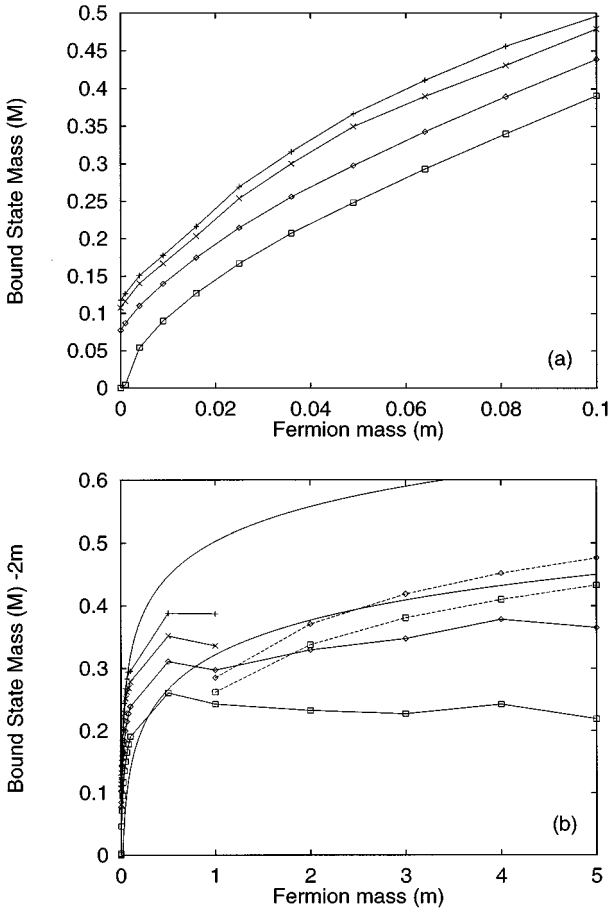

FIG. 7. (a) shows bound state masses (M) against fermion mass 0–0.1. (b) is a plot of $M-2m$ for $m=0$–5. In each plot the scalar $\mathscr{C}=+1$ ($\diamond$), scalar $\mathscr{C}=-1$ ($+$), axiscalar $\mathscr{C}=+1$ ($\square$), and axiscalar $\mathscr{C}=-1$ ($\times$) states are drawn with solid curves. The nonrelativistic predictions of Eq. (3.20) and Eq. (3.21) are the scalar $\mathscr{C}=+1$ ($\diamond$) and axiscalar $\mathscr{C}=+1$ ($\square$) states, respectively, and are drawn with dashed lines. Equation (3.2) with $\lambda=\lambda_0$ (lower solid curve with no symbols) and with λ_1 (upper solid curve with no symbols) are also plotted in (b).

genvalue Λ of Eq. (2.13) is 1. This was repeated for each of the fermion masses ranging from 0 to 5.0. This procedure was used for each of the four nondegenerate bound state symmetries described in the Appendix.

Table II shows the bound state masses for each of the four symmetries (scalar $\mathscr{C}=+1$, scalar $\mathscr{C}=-1$, axiscalar $\mathscr{C}=+1$, and axiscalar $\mathscr{C}=-1$) for all fermion masses considered. Figure 7(a) displays the solutions M for fermion mass 0–0.1. Figure 7(b) shows $M-2m$ over the greater range of 0–5. The axiscalar $\mathscr{C}=+1$ solution is a degenerate axiscalar-axipseudoscalar pair of Goldstone bosons for the case $m=0$, as seen in previous work [4]. Minor differences between Ref. [4] and the current work at $m=0$ are due to small differences in the propagator fits, as explained in Sec. IV.

For small m the bound state masses rise rapidly with with increasing fermion mass. The mass of the ''Goldstone'' axiscalar $\mathscr{C}=+1$ state scales roughly with the square root of the fermion mass, in agreement with the Gell-Mann–Okubo mass formula [14]. In fact, for fermion masses 0 to 0.1 a linear regression against $\sqrt{m}$ has correlation coefficient 0.9964 with the mass growing as approximately $1.27\times\sqrt{m}$. [The accuracy of the solution at $m=0.001$, which comes out with an anomalously low bound state mass, is severely affected by numerical inaccuracy arising from the sensitivity the bound state mass to the eigenvalue Λ in Eq. (2.13).] For large fermion masses, the bound state mass rises predominantly as twice the fermion mass plus possible logarithmic corrections. However, there appears to be a good deal of noise in the large m solutions, reflecting the difficulty in accurately modeling the fermion propagator deep into the timelike region from spacelike fits. No solutions corresponding to states of negative charge parity were found for $m>1.0$.

Numerical solutions to the integral equations (3.20), (3.21) arising from our non-relativistic treatment are listed in Table III and plotted in Fig. 7(b). Solutions with positive δ were found for fermion masses $m\geqslant 1.0$ in the positive charge parity sector. We were unable to locate any solutions to Eqs. (3.20) and (3.21) corresponding to negative charge parity states over a broad range of δ. Also given in Table III and Fig. 7(b) are the two lowest lying s-wave solutions to the Schrödinger equation from the numerical work of Tam *et al.* [9], given by Eq. (3.2).

The lack of exact agreement between the nonrelativistic,

one-loop approximations Eqs. (3.20) and (3.21), and the Schrödinger equation result Eq. (3.2) is to be expected. As pointed out in Sec. III, a complete cancellation of infrared divergences can only occur if the fermion self-energy is calculated nonperturbatively to all orders. From Table III, we see that at very high fermion masses, the accuracy of the one-loop approximation is significantly affected as the conjugate poles in the propagator, measured in momenta scaled by the fermion mass, move closer to the bare fermion mass pole (see Fig. 2). At more moderate fermion masses, $m \approx 5$, the one-loop approximation is more respectable.

We see no clear agreement between the numerical results of Eq. (2.7), and either nonrelativistic approximation Eqs. (3.20), (3.21), or the Schrödinger equation result Eq. (3.2). Our analysis of the nonrelativistic limit of the BS equation exposes the importance of the analytic structure of the fermion propagator in the vicinity of the bare fermion mass pole $p^2 = -m^2$. The uneven nature of the lower two curves in Fig. 7(b) indicates that the determination of the timelike fermion propagator by an analytic fit to the spacelike propagator is inadequate for fermion masses $m \geqslant 1$. It is clear that a more careful analysis of the timelike nature of the fermion propagator, possibly involving a fully nonperturbative treatment of the SD equation to include remnant chiral symmetry breaking, is necessary for determining the bound state spectrum for even moderately large fermion masses.

It is important to note that the poles in the fermion propagator fits listed in Table I lie outside the BS integration region Ω for all solutions obtained. This can be verified by observing that all masses in Table II are lower than the values $M_{\max}$ listed in Table I. A similar situation arises for the non-relativistic limit calculations. Listed in Table III are maximum allowed δ values if the integration region sampled by Eqs. (3.20) and (3.21) is not to impinge on the conjugate propagator poles q_3^{pole} and $(q_3^{\text{pole}})^*$ defined in Eq. (3.24). In all cases the numerical results lie within the permitted region. This requirement is equivalent to demanding that q_3^{pole} should not cross the real q_3 axis as as $|\mathbf{q}|$ ranges from 0 to ∞. Interestingly, such a crossing would entail a more careful evaluation of residues than that carried out in Sec. III leading to the Schrödinger equation.

We note that the Schrödinger equation results of Ref. [9] include the first five s-wave states. It would certainly be of interest to locate the excited states within the framework of our BS treatment of QED_3. We have searched for solutions to the eigenvalue equation (2.13) corresponding to excited states, and find in general no solutions within the mass ranges allowed by the values $M_{\max}$ in Table I. Since there is no reason to assume that the s-wave spectrum should be bounded above, it seems likely that there will be solutions to the BS equation for which the region of integration Ω does include the conjugate propagator poles discussed in Sec. IV. It follows that the functions f, U, V, and W in the BS amplitudes of these states should have compensating zeros, in order that the right-hand side of the BS equation be integrable. We conjecture that, if the fermion propagator has an infinite set of poles, there will be a sequence of excited states, the nth excited state having n pairs of zeros in its BS amplitude. This conjecture is consistent with the the first excited state of the Schrödinger equation, also listed in Table III, for which the wave function has a single zero.

Although we are unable to determine accurately the spectrum in the large fermion mass limit, our calculations strongly suggest that there are no scalar or axiscalar states with negative charge parity in this limit. This is consistent with the nonrelativistic quark model in four dimensions in which negative charge parity scalar and pseudoscalar states are forbidden by the generalized Pauli exclusion principle [14]. We note, however, that there is nothing to exclude such states in a fully relativistic BS treatment [15], and indeed, negative charge parity scalar and axiscalar states are found within the current model for light fermions.

TABLE II. Bound state masses for fermion masses from 0 to 5.0. (All masses ± 0.001 unless otherwise stated.) The axiscalar $\mathscr{C} = +1$ solution with $m = 0$ stated here is an analytic result.

m	Scalar $\mathscr{C} = +1$	Scalar $\mathscr{C} = -1$	Axiscalar $\mathscr{C} = +1$	Axiscalar $\mathscr{C} = -1$
0 (Ref. [4])	0.080 ± 0.001	0.123 ± 0.002	0	0.111 ± 0.002
0	0.077	0.118	0	0.108
0.001	0.087	0.126	0.004	0.116
0.004	0.110	0.151	0.054	0.140
0.009	0.140	0.178	0.090	0.167
0.016	0.175	0.217	0.127	0.204
0.025	0.215	0.269	0.167	0.254
0.036	0.256	0.316	0.208	0.300
0.049	0.298	0.367	0.248	0.350
0.064	0.343	0.411	0.293	0.390
0.081	0.389	0.456	0.340	0.431
0.1	0.439	0.496	0.391	0.479
0.5	1.311	1.388	1.261	1.352
1	2.297	2.387	2.243	2.336
2	4.330	–	4.233	–
3	6.348	–	6.227	–
4	8.379	–	8.243	–
5	10.365	–	10.219	–

VI. CONCLUSIONS

In this paper we have solved the combination of rainbow Schwinger-Dyson and homogeneous Bethe-Salpeter equations in the quenched ladder approximation for three-dimensional QED with massive fermions. QED_3 was chosen because, like QCD, it is confining but without the complications of being non-Abelian. A four-component version of this theory is used because, also like QCD, it provides a parity invariant action with a spontaneously broken chiral-like symmetry in the massless limit. The approximation is amenable to numerical solution, and should help assess the limitations of a technique frequently employed in models of QCD [2].

The work in this paper carries on from a previous study of the same subject [4], but with the following extensions. First, nonzero fermion mass is considered. Second, an analysis of the fermion propagator in the complex plane is carried out in order to assess the appropriateness of the approximations involved. Thirdly, an analysis of the nonrelativistic limit, i.e., large bare fermion mass, is made in an attempt to compare with existing Schrödinger equation studies of QED_3.

The rainbow SD equation was solved in Euclidean space to give a fermion propagator for spacelike momenta, Euclidean $p^2>0$. The propagator is chirally asymmetric, and in the massless fermion limit, gives rise to a doublet of massless Goldstone positronium states analogous to the pion. Solution of the BS equation for massive positronium states requires knowledge of the fermion propagator $S(p)$ in the complex p^2 plane extending away from the spacelike axis, and a finite distance into the timelike axis $p^2<0$. By rotating the contour of integration we were able to extend the spacelike solution into part of the complex plane. However, the occurrence of complex conjugate poles in the fermion propagator prevented a numerical solution to the SD equation throughout the complete region of the complex plane sampled by the BS equation. This forced us to apply analytic fits to the propagator along the positive real p^2 axis for use over the required part of the complex plane.

Our propagator fits were found to have conjugate poles located close to those of the direct solution for small to moderate fermion masses. This, combined with the accuracy of the fits throughout much the complex p^2 plane, made our choice of propagator very attractive. The singularities in the fits were found to move onto the negative real p^2 axis as the fermion mass increased. This was not interpreted as a loss of confinement but instead attributed to a lack of accuracy in the fits deep into the timelike region as the fermion mass became large. This reduction in accuracy of the fits for large m was due to the nature of the functions along the positive real p^2 axis where the fits were made, and the presence of a singularity near the negative real p^2 axis in the vicinity of the bare fermion mass pole $p^2=-m^2$, but off the timelike axis.

BS solutions were found for four pairs of parity degenerate states. These pairs were the scalar-pseudoscalar $\mathscr{C}=+1$ and $\mathscr{C}=-1$ and the axiscalar-axipseudoscalar $\mathscr{C}=+1$ and $\mathscr{C}=-1$ states. For small to moderate fermion mass the bound state mass was found to increase smoothly with m. The axiscalar $\mathscr{C}=+1$ doublet, analogous to the pion, was the lowest in energy, with a mass rising roughly with the square root of the bare fermion mass. For moderately large bare fermion masses (m/e^2 greater than unity) the positronium masses rise as twice the bare fermion mass, plus a possible logarithmic correction. However, an unacceptable level of noise was found to develop in our results for these larger masses, which we attribute to inaccuracies in the analytically continued fermion propagators in the important region near the bare fermion mass pole. No negative charge parity ($\mathscr{C}=-1$) solutions were found for bare fermion masses above $m/e^2\approx 1.0$, consistent with the generalized Pauli exclusion principle of nonrelativistic QCD_4.

TABLE III. Nonrelativistic δ solutions for positive charge parity, from Eqs. (3.20), and (3.21) and the two lightest s-wave Schrödinger equation results of Tam *et al.* [9], Eq. (3.2) using $\lambda_0=1.7969$ and $\lambda_1=2.9316$. The first column contains the maximum values of δ allowed before conjugate singularities arise in the fermion propagator used in our nonrelativistic calculations.

m	$\delta_{\max}$	Scalar Eq. (3.20)	Axiscalar Eq. (3.21)	Eq. (3.2) with $\lambda=\lambda_0$	Eq. (3.2) with $\lambda=\lambda_1$
1	0.332	0.285	0.262	0.322	0.503
2	0.421	0.371	0.338	0.377	0.558
3	0.473	0.419	0.381	0.409	0.590
4	0.511	0.452	0.410	0.432	0.613
5	0.540	0.476	0.433	0.450	0.631
100	0.947	0.792	0.734	0.688	0.869
1000	1.272	1.030	0.968	0.872	1.052

The conjugate poles in the fermion propagators were found to keep clear of the integration regions required for the BS solutions for the lowest state in each of the four space-parity−charge-parity sectors considered. However, it appeared that this would not be so for any excited states. We therefore conjecture that the excited positronium states have zeros in their BS amplitudes positioned so as to cancel the poles in the propagators encountered within the integral in the BS equation (2.1). This requirement of compensating zeros was too demanding on our current numerical code, and as a result, no excited states were found.

In vector calculations under way at present, where the bound state masses are expected to be larger, the conjugate poles in the fermion propagator seen in this work may interfere. Since the fits used in this work appear to have their singularities close to those in the actual Schwinger-Dyson solution, we may find that the rainbow approximation and the resulting propagator fits will be inadequate for a study of vector states in QED_3. This is a very challenging problem and we hope to report on our results in the near future.

A nonrelativistic analysis of the BS equation was also carried out assuming, in the first instance, a one-loop approximation to the fermion propagator. However it was shown that, in order to cancel infrared divergences completely between the photon propagator and fermion self energy, as proposed by Sen [10] and Cornwall [11], it is necessary to evaluate the fermion self-energy nonperturbatively. Only if this is done can the Schrödinger equation be rigorously obtained in the large fermion mass limit. In spite of this, numerical solutions of the one-loop equations give reasonable agreement with the Schrödinger equation for moderately large fermion masses $m/e^2\approx 5$.

In summary, we were able to carry out an acceptable analysis of the bound state spectrum of QED_3 near the chiral

limit $m \to 0$ by using analytic fits to the spacelike fermion propagators in the BS Bethe-Salpeter equation, and in the nonrelativistic limit $m \to \infty$ by expanding to lowest order in inverse powers of the fermion mass to obtain a Schrödinger equation. However, there remains an intermediate mass range $m/e^2 \approx 1$ for which neither of these techniques is adequate. It is clear that a more careful non-perturbative analysis of the fermion propagator in the vicinity of the bare fermion mass pole is necessary before an accurate determination of the QED_3 positronium spectrum at intermediate fermion masses can be made. If a direct analogy with QCD models based on the Bethe-Salpeter equations is made, we conclude that particular care must be taken in modeling quark propagators for quarks whose mass is close to the mass scale of the theory, namely charm quarks.

ACKNOWLEDGMENTS

We are grateful to C. J. Hamer, A. Tam and P. Maris for helpful discussions, and the National Centre for Theoretical Physics at the Australian National University for hosting the Workshop on Non-Perturbative Methods in Field Theory where part of this work was completed.

APPENDIX: TRANSFORMATION PROPERTIES IN QED_3

The four-component QED_3 action in Minkowski space [16]

$$S[A,\overline{\psi},\psi] = \int d^3x [-\tfrac{1}{4} F_{\mu\nu} F^{\mu\nu} + \overline{\psi}\,\gamma_\mu (i\partial^\mu + eA^\mu)\psi + m\overline{\psi}\,\psi], \tag{A1}$$

involves 4×4 matrices γ_μ which satisfy $\{\gamma_\mu,\gamma_\nu\} = 2\eta_{\mu\nu}$ where $\eta_{\mu\nu} = \mathrm{diag}(1,-1,-1)$ with $\mu = 0$, 1, and 2. These three matrices belong to a complete set of 16 matrices $\{\gamma_A\} = \{I, \gamma_4, \gamma_5, \gamma_{45}, \gamma_\mu, \gamma_{\mu 4}, \gamma_{\mu 5}, \gamma_{\mu 45}\}$ satisfying $(1/4)\mathrm{tr}(\gamma_A \gamma^B) = \delta_A^B$:

$$\gamma_0 = \begin{pmatrix} \sigma_3 & 0 \\ 0 & -\sigma_3 \end{pmatrix}, \quad \gamma_{1,2} = -i \begin{pmatrix} \sigma_{1,2} & 0 \\ 0 & -\sigma_{1,2} \end{pmatrix},$$

$$\gamma_4 = \gamma^4 = \begin{pmatrix} 0 & I \\ I & 0 \end{pmatrix},$$

$$\gamma_5 = \gamma^5 = \begin{pmatrix} 0 & -iI \\ iI & 0 \end{pmatrix},$$

$$\gamma_{45} = \gamma^{45} = -i\gamma_4\gamma_5,$$

$$\gamma_{\mu 4} = i\gamma_\mu\gamma_4,$$

$$\gamma_{\mu 5} = i\gamma_\mu\gamma_5,$$

$$\gamma_{\mu 45} = -i\gamma_\mu\gamma_4\gamma_5,$$

$$\gamma^{\mu 4, \mu 5 \text{ or } \mu 45} = \eta^{\mu\nu}\gamma_{\nu 4, \nu 5 \text{ or } \nu 45}.$$

The three γ_μ, and γ_4 and γ_5 are five mutually anticommuting matrices. This is unlike the four-dimensional case where no analogue of γ_4 exists.

The action Eq. (A1) in the massless case $m = 0$ exhibits global U(2) symmetry with generators $\{I, \gamma_4, \gamma_5, \gamma_{45}\}$ which is broken by the generation of a dynamical fermion mass [17,16] to a $U(1)\times U(1)$ symmetry $\{I, \gamma_{45}\}$. The action is also invariant with respect to discrete parity and charge conjugation symmetries, which for the fermion fields are given by

$$\psi(x) \to \psi'(x') = \Pi\psi(x), \quad \overline{\psi}(x) \to \overline{\psi}'(x') = \overline{\psi}(x)\Pi^{-1}, \tag{A2}$$

$$\psi(x) \to \psi'(x) = C\overline{\psi}(x)^T, \quad \overline{\psi}(x) \to \overline{\psi}'(x) = -\psi(x)^T C^\dagger, \tag{A3}$$

where $x' = (x^0, -x^1, x^2)$. The matrices Π and C are each determined only up to an arbitrary phase by the condition that the action Eq. (A1) be invariant [4]:

$$\Pi = \gamma_{14} e^{i\phi_P \gamma_{45}}, \quad C = \gamma_2 e^{i\phi_C \gamma_{45}} \quad (0 \leqslant \phi_P, \phi_C < 2\pi). \tag{A4}$$

Scalars, pseudoscalars, axiscalars, and axipseudoscalars are defined by the following transformation properties under parity transformations:

$$\Phi^S(x) \to \Phi^{S\prime}(x') = \Phi^S(x),$$

$$\Phi^{PS}(x) \to \Phi^{PS\prime}(x') = -\Phi^{PS}(x),$$

$$\Phi^{AS}(x) \to \Phi^{AS\prime}(x') = R_P \Phi^{AS}(x),$$

$$\Phi^{APS}(x) \to \Phi^{APS\prime}(x') = -R_P \Phi^{APS}(x), \tag{A5}$$

where Φ^{AS} and Φ^{APS} are doublet states $\Phi = (\Phi_4, \Phi_5)^T$, and

$$R_P = \begin{pmatrix} -\cos 2\phi_P & -\sin 2\phi_P \\ -\sin 2\phi_P & \cos 2\phi_P \end{pmatrix}. \tag{A6}$$

Similar transformation properties exist for charge conjugation.

The most general forms of the Bethe-Salpeter amplitudes [15] for bound scalar and pseudoscalar states are

$$\Gamma^S(q,P) = If + \not{q} g + \not{P} h + \epsilon_{\mu\nu\rho} P^\mu q^\nu \gamma^{\rho 45} k, \tag{A7}$$

$$\Gamma^{PS}(q,P) = \gamma_{45}\Gamma^S(q,P), \tag{A8}$$

where f, g, h, and k are functions only of q^2, P^2, and $q\cdot P$. BS amplitudes corresponding to the components Φ_4 and Φ_5 of axiscalars and axipseudoscalars take the general form

$$\begin{pmatrix} \Gamma^{(4)}(q,P) \\ \Gamma^{(5)}(q,P) \end{pmatrix}^{AS} = \begin{pmatrix} \gamma_4 \\ \gamma_5 \end{pmatrix} f + \begin{pmatrix} \gamma_{\mu 4} \\ \gamma_{\mu 5} \end{pmatrix} (q^\mu g + P^\mu h) + \epsilon_{\mu\nu\rho} P^\mu q^\nu \begin{pmatrix} \gamma^{\rho 5} \\ -\gamma^{\rho 4} \end{pmatrix} k, \tag{A9}$$

and

$$\begin{pmatrix} \Gamma^{(4)}(q,P) \\ \Gamma^{(5)}(q,P) \end{pmatrix}^{APS} = \gamma_{45} \begin{pmatrix} \Gamma^{(4)}(q,P) \\ \Gamma^{(5)}(q,P) \end{pmatrix}^{AS}. \qquad \text{(A10)}$$

Furthermore, the charge parity $\mathscr{C} = \pm 1$ of the bound states is determined by the parity of the functions f, g, h, and k under the transformation $q \cdot P \to -q \cdot P$. The quantity $q \cdot P$ is the only Lorentz invariant which changes sign under charge conjugation and thus determines the charge parity of those functions.

Our conventions for Euclidean space quantities are summarised in Appendix A of Ref. [4]. In particular Euclidean momenta and Dirac matrices are defined by

$$P_3^{(E)} = -iP_0^{(M)}, \quad P_{1,2}^{(E)} = P_{1,2}^{(M)}, \quad \gamma_3^{(E)} = \gamma_0^{(M)},$$

$$\gamma_{1,2}^{(E)} = i\gamma_{1,2}^{(M)}.$$

[1] C. J. Burden, J. Praschifka, and C. D. Roberts, Phys. Rev. D **46**, 2695 (1992).

[2] J. Praschifka, C. D. Roberts, and R. T. Cahill, Int. J. Mod. Phys. A **4**, 4929 (1989); Y.-B. Dai, C.-S. Huang, and D.-S. Liu, Phys. Rev. D **43**, 1717 (1991); K.-I. Aoki, T. Kugo, and M. G. Mitchard, Phys. Lett. B **266**, 467 (1991); H. J. Munczek and P. Jain, Phys. Rev. D **46**, 438 (1992); P. Jain and H. J. Munczek, *ibid.* **48**, 5403 (1993); C. J. Burden, *et al.* (unpublished); R. T. Cahill and S. T. Gunner, Phys. Lett. B **359**, 281 (1995).

[3] S. J. Stainsby and. R. T. Cahill, Mod. Phys. Lett. A **9**, 3551 (1994).

[4] C. J. Burden, Nucl. Phys. **B387**, 419 (1992).

[5] P. Maris, Ph.D. thesis, Rijkunivsiteit, Groningen, 1993.

[6] P. Maris, Phys. Rev. D **52**, 6087 (1995).

[7] R. Delbourgo and. M. Scadron, J. Phys. G **5**, 1621 (1979).

[8] C. M. Yung and C. J. Hamer, Phys. Rev. D **44**, 2595 (1991).

[9] A. Tam, C. J. Hamer, and C. M. Yung, J. Phys. G **21**, 1463 (1995); see also V. G. Koures, ''Solving the Coulomb Schrödinger equation in $d=2+1$ via sinc collocation,'' University of Utah Report No. UTAH-IDR-CP-05 (unpublished).

[10] D. Sen, Phys. Rev. D **41**, 1227 (1990).

[11] J. M. Cornwall, Phys. Rev. D **22**, 1452 (1980).

[12] C. D. Roberts and A. G. Williams, Prog. Part. Nucl. Phys. **33**, 475 (1994).

[13] S. J. Stainsby and. R. T. Cahill, Int. J. Mod. Phys. A **7**, 7541 (1992).

[14] D. Flamm and F. Schöberl, *Introduction to the Quark Model of Elementary Particles* (Gordon and Breach, New York, 1982).

[15] C. H. Llewellyn Smith, Ann. Phys. (N.Y.) **53** (1969) 521; Llewellyn Smith's vertex χ is related to our vertex Γ via $\chi[(1/2)P,q] = S[(1/2)P+q]\Gamma(q,P)S[(1/2)P-q]$.

[16] R. D. Pisarski, Phys. Rev. D **29**, 2423 (1984).

[17] E. Dagotto, J. B. Kogut, and A. Kocic, Phys. Rev. Lett. **62**, 1083 (1989); Nucl. Phys. **B334**, 279 (1990).